Origin of Enhanced Hole Injection in Inverted Organic Devices with Electron Accepting Interlayer

*Cephas E. Small, Sai-Wing Tsang, Junji Kido, Shu Kong So, and Franky So**

Conventional organic light emitting devices have a bottom buffer interlayer placed underneath the hole transporting layer (HTL) to improve hole injection from the indium tin oxide (ITO) electrode. In this work, a substantial enhancement in hole injection efficiency is demonstrated when an electron accepting interlayer is evaporated on top of the HTL in an inverted device along with a top hole injection anode compared with the conventional device with a bottom hole injection anode. Current–voltage and space-charge-limited dark injection (DI-SCLC) measurements were used to characterize the conventional and inverted *N*,*N*′-diphenyl-*N*,*N*′-bis(1-naphthyl)(1,1′biphenyl)-4,4′diamine (NPB) hole-only devices with either molybdenum trioxide (MoO_3) or 1,4,5,8,9,11-hexaazatriphenylene hexacarbonitrile (HAT-CN) as the interlayer. Both normal and inverted devices with HAT-CN showed significantly higher injection efficiencies compared to similar devices with MoO_3, with the inverted device with HAT-CN as the interlayer showing a *hole injection efficiency close to 100%*. The results from doping NPB with MoO_3 or HAT-CN confirmed that the injection efficiency enhancements in the inverted devices were due to the enhanced charge transfer at the electron acceptor/NPB interface.

1. Introduction

Research aimed at optimizing the performance of organic light-emitting diodes (OLEDs) has received much attention in recent years due to the enormous potential of the technology in flat panel display and solid state lighting applications.[1] A key requirement to demonstrating OLEDs with efficient operation is to optimize carrier injection from the electrodes to the active emitting layer.[2,3] This requirement is due to the low intrinsic carrier concentration of organic semiconductors and thus the need to reduce the device operating voltage. Optimizing carrier injection is not a simple task, especially since OLEDs utilize wide band-gap materials whose energy levels do not match the work-function of the electrodes. The work function mismatch is especially a problem for hole injection because the work function of transparent electrodes such as indium tin oxide (ITO) is less than 5.0 eV while the highest occupied molecular orbital (HOMO) energies of wide band-gap hole transporting materials commonly used in OLEDs are typically 5.5 eV or higher, resulting in low hole injection efficiencies.

To overcome this limitation, interlayers are often incorporated into the device to enhance hole injection. For conventional OLEDs with a bottom ITO contact, materials used for the hole-injecting interlayer can be grouped into two categories. One class of materials used for the hole injecting interlayer is conducting polymers, such as poly(3,4-ethylenedioxythiophene) poly(styrenesulfonate) (PEDOT:PSS).[4–6] Although the use of PEDOT:PSS as a hole injection layer (HIL) has been quite popular in small-molecule and polymer OLED research, its work-function of 5.0 eV is not adequate to provide optimum hole injection into wide band-gap materials with a deep HOMO energy.[7] Another class of materials used as interlayer is strong electron acceptors. These materials can facilitate enhanced hole injection in OLEDs.[8] Unlike conducting polymer HILs, electron accepting interlayers modify the energy levels of the anode and wide band-gap hole transporting materials when inserted between these two layers. For example, previously reported ultraviolet photoemission spectroscopy (UPS) results showed that the strong electron-accepting nature of MoO_3 was responsible for both the large vacuum level shift in the anode indium tin oxide (ITO) and the observed band-bending in the HOMO level of the hole-transporting layer.[9] Similar results were also found for organic acceptors such as HAT-CN.[10,11] The strong band-bending of the hole-transporting layer's HOMO level is indicative that the Fermi level moves down and pins at a certain position as typical for *p*-doping. The use of electron acceptors for controlled *p*-doping in amorphous hole-transporting materials employed in high efficiency OLEDs has been well studied.[12–18] For example, strong *p*-type doping has also been observed when MoO_3 was used as a dopant in hole transporters with a deep HOMO level.[16] Due to their ability to modify the energy levels of the anode and the wide band-gap hole transporting layers,

Prof. J. Kido
Department of Organic Device Engineering
Yamagata University
Yonezawa, Yamagata 992-8510, Japan
Prof. S. K. So
Department of Physics
Hong Kong Baptist University
Kowloon, Hong Kong
C. E. Small, Dr. S.-W. Tsang, Prof. F. So
Department of Materials Science and Engineering
University of Florida
Gainesville, FL 32611 USA
E-mail: fso@mse.ufl.edu

DOI: 10.1002/adfm.201200185

these electron acceptors can serve as efficient hole injectors for wide band-gap materials with a deep HOMO level.

Despite the use of conducting polymers or electron acceptors as interlayers for improved carrier injection in organic devices, truly ohmic hole injection has rarely been reported. When the hole injection contact is ohmic, the carrier transport is limited by the bulk of the materials rather than the injection contact. As a result of the ohmic injection, the carrier transport is space-charge limited.[13] The determination between bulk-limited versus injection-limited transport is made by calculating the carrier injection efficiency, which is the ratio between the measured steady-state current density of the device and the theoretical space-charge-limited current density given by Child's Law.[19] Even for conventional bottom-injection contact hole-only devices with PEDOT:PSS as an interlayer, injection-limited transport and low injection efficiency values ranging from 30 to 60% have been reported.[7] Additional studies featuring MoO_3 as an electron accepting interlayers have reported even lower injection efficiencies for similar single-carrier devices.[20] Recently, two novel approaches have been demonstrated for achieving ohmic hole injection in OLEDs. One approach is to utilize a composite HIL consisting of a mixture of conducting polymers with different work functions and graphene for ohmic hole injection in flexible OLEDs.[21] The other approach for achieving ohmic hole injection consists of using electron accepting interlayers in OLEDs with an inverted architecture, with a substantial enhancement in current density being observed in the device when the bottom hole injection contact using PEDOT:PSS interlayer is replaced by a top hole injection contact using MoO_3 interlayer.[22] In these inverted devices, the electron accepting interlayer is deposited on top of the hole transporting layer to form the top hole injection contact. Using this approach, optimized hole injection into wide band-gap materials can be achieved. However, the origin of this enhancement is not understood.

In this work, the mechanism of enhanced hole injection in inverted organic devices with different electron accepting interlayers is investigated. Our results suggest a generalized behavior of the electron acceptors MoO_3 and HAT-CN to provide enhanced hole injection in devices with an inverted architecture. A widely used amorphous hole transporting material *N,N'*-di(naphthalene-1-yl)-*N,N'*-diphenyl-benzidine (NPB), was used for this study.[23–25] Current-voltage (*J-V*) and space-charge-limited dark injection (DI-SCLC) transient measurements were used to characterize the hole injection efficiency in the normal and inverted single-carrier devices. We found that HAT-CN is a superior hole injector compared with MoO_3 as a hole injection interlayer used in both normal and inverted devices. Furthermore, we found that the inverted devices with a top hole injection contact showed a higher injection efficiency compared to the normal devices with a bottom injection contact. For inverted devices with top-contact HAT-CN interlayer truly ohmic hole injection was demonstrated, with an injection efficiency close to 100% being obtained. We believe this injection efficiency is the highest reported for NPB in the literature to date. These results suggest that a better charge transfer at the electron acceptor/NPB interface is formed in the inverted device architecture. In this work, the term 'charge transfer' refers to the transfer of electrons from the HOMO of NPB to the lowest unoccupied molecular orbital (LUMO) of the electron acceptor as discussed in previous photoemission spectroscopy results for MoO_3 and HAT-CN.[9–11] To further support our charge transfer model, we fabricated normal NPB single-carrier devices that consisted of either a neat MoO_3 HIL or a MoO_3-doped NPB injection layer. Not only did we observe enhanced hole injection for devices with a MoO_3-doped NPB injection layer, but we also found that the injection efficiency can be tuned by increasing the MoO_3 doping concentration. Lastly, to understand why HAT-CN was the better hole injector compared to MoO_3, we fabricated hole-only devices with a *p*-doped NPB interlayer using both electron acceptors as dopants. The doping effect obtained using a fixed doping concentration of HAT-CN or MoO_3 in NPB allowed us to characterize the degree of charge transfer between the electron acceptors and NPB. Since stonger p-type doping was observed when HAT-CN was used as the dopant compared with MoO_3, we confirmed that HAT-CN provides more efficient charge transfer with NPB compared to MoO_3.

2. Results and Discussion

2.1. *J–V* Characterization and Injection Efficiency

Normal and inverted hole-only devices were fabricated for this work. The hole injection behavior of NPB single-carrier devices with electron accepting HILs were analyzed by *J–V* characterization. Assuming that the organic material is trap free with an ohmic injection contact, the steady-state current should follow the space-charge-limited current (J_{SCL}) as follows:[26]

$$J_{SCL} = \frac{9}{8}\mu_0\varepsilon_0\varepsilon_r \exp\left(0.89\beta\sqrt{F}\right)\frac{F^2}{d} \quad (1)$$

where μ_0 is the zero-field mobility, ε_0 is the vacuum permittivity, ε_r is the relative permittivity, and $F = V/d$ is the applied electric field. The Poole-Frenkel slope β is the field-dependent mobility coefficient. Both $\beta = 1.3 \times 10^{-3}$ $(cm/V)^{-1/2}$ and $\mu_0 = 2.7 \times 10^{-4}$ cm^2/V s were obtained from independent time-of-flight (TOF) measurements reported in the literature.[20]

Figure 1a shows the current density vs. electric field characteristics for the normal and inverted NPB hole-only devices with either MoO_3 or HAT-CN as the HIL. The solid line shown in Figure 1a represents the theoretical J_{SCL} calculated from Equation 1. Two conclusions can be drawn directly from these results. First, the inverted NPB hole-only devices showed enhanced current densities compared to the devices with the normal architecture with MoO_3 or HAT-CN as the HIL. Second, the devices with HAT-CN HIL showed a significantly a larger current density than similar devices using MoO_3 as the HIL. It should be noted that the inverted NPB device with HAT-CN HIL was the only device to show a good agreement with the theoretical J_{SCL} curve. The injection efficiency, η_{INJ}, was then calculated from the *J-V* characteristics:[19]

$$\eta_{INJ} = J_{INJ}/J_{SCL} \quad (2)$$

where J_{INJ} is the measured steady-state current density and J_{SCL} is the calculated theoretical space-charge-limited current density. The hole injection efficiencies η_{INJ} as a function of electric

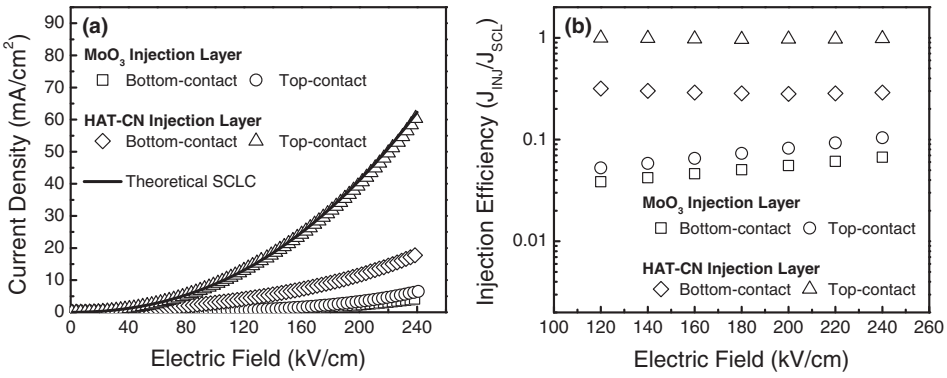

Figure 1. a) Current density vs. electric field for NPB hole-only devices using either MoO_3 or HAT-CN as HIL in a normal or inverted device architecture. Solid line represents theoretical J_{SCL}. b) Hole injection efficiency as a function of electric field for the devices.

field for the devices are shown in Figure 1b. A marked improvement in hole injection efficiencies was observed for the inverted devices with either a MoO_3 or HAT-CN HIL compared to the normal device. The injection efficiency for inverted devices with HAT-CN top-contact HIL is near unity, meaning that the injection contact is truly ohmic. These results show that improved hole injection in inverted NPB hole-only devices using MoO_3 or HAT-CN as HIL is a generalized behavior.

2.2. Space-Charge-Limited Dark Injection Transient Measurement

Analysis of the DI-SCLC transient data provides in-depth understanding of the charge injection processes.[19,20] **Figure 2**a and b shows the DI-SCLC transients with increasing applied bias for normal and inverted NPB single carrier devices with MoO_3 injection layer. The measured transients show a well-defined maximum, representing the leading front of the injected carriers transporting to the non-injecting electrode, followed by decay to a saturation value. The position of the maximum in time, τ_{DI}, is related to the transient time by $\tau_{DI} \approx 0.8\tau_{tr}$. The shift in τ_{DI} to shorter times with increasing applied bias indicates that the hole mobility in NPB is field dependent.[7] Larger current density values can be observed in the inverted hole-only devices compared to normal devices with the same film thickness. A similar result was obtained from DI-SCLC transients of normal and inverted NPB single carrier devices with HAT-CN HIL, shown in **Figure 3**a and b respectively. These devices showed larger transient current densities compared to the corresponding devices with MoO_3 HIL, which is consistent with the *J-V* measurements highlighted in Section 2.1. Furthermore, we confirmed that HAT-CN HIL provides ohmic hole injection in inverted NPB devices by calculating hole injection efficiencies based on the DI-SCLC transient measurements, which show $\eta_{INJ} \approx 1$ for devices with top-contact HAT-CN HIL (see Supporting Information, Figure S1).

Analyzing all of the normal and inverted NPB hole-only devices under the same applied field revealed a difference in the measured τ_{DI}. DI-SCLC transient measurements assume the injection contact for the device is truly ohmic. If the injection contact is injection limited, then the carrier mobility calculated from the transients (μ_{DI}) will be limited since the transient time corresponding to the leading front charge (τ_{DI}) will be delayed due to inefficient charge injection. Since the injection contact for our inverted device with HAT-CN HIL was truly ohmic while the injection contacts corresponding to the other devices were somewhat injection-limited, the measured τ_{DI} for

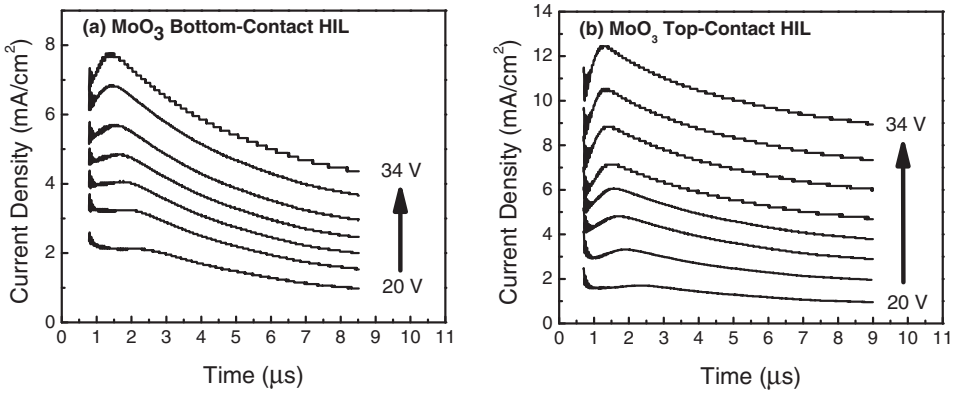

Figure 2. DI-current density transients measured at various applied voltages using MoO_3 as HIL in a a) normal device architecture and an b) inverted device architecture.

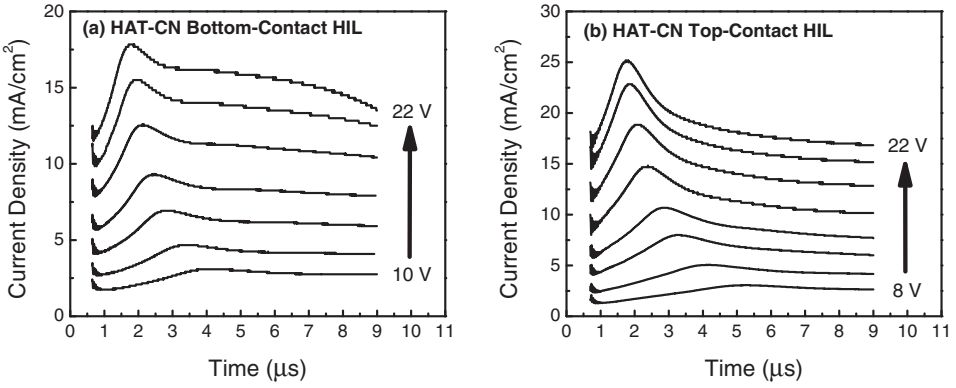

Figure 3. DI-current density transients measured at various applied voltages using HAT-CN as HIL in a a) normal device architecture and an b) inverted device architecture.

the inverted device with HAT-CN HIL was shorter than those obtained for the other devices. From the measured DI-SCLC transients for these devices, the carrier mobility μ_{DI} were calculated as follows:[27]

$$\mu_{DI} = \frac{0.787d^2}{\tau_{DI} \cdot V} \quad (3)$$

where d is the thickness of the organic layer and V is the voltage applied to the sample. Using Equation 3, the carrier mobility was plotted as a function of electric field for each of the normal and inverted NPB devices with either MoO_3 or HAT-CN HIL (see **Figure 4**). The field-dependent mobility values extracted from previously reported time-of-flight (TOF) measurements are shown for comparison.[28] The extracted hole mobility for the devices correlated very well with the measured injection efficiencies. Devices with higher injection efficiency showed a larger μ_{DI} under the same applied field. The mobility values for inverted device with HAT-CN HIL are in good agreement with previously reported time-of-flight (TOF) mobility values measured at the same applied electric field for NPB single-carrier devices.[20,28] These results provide further evidence that inverting the device architecture when using electron acceptors as HILs is necessary to improve hole injection into organic electronic devices.

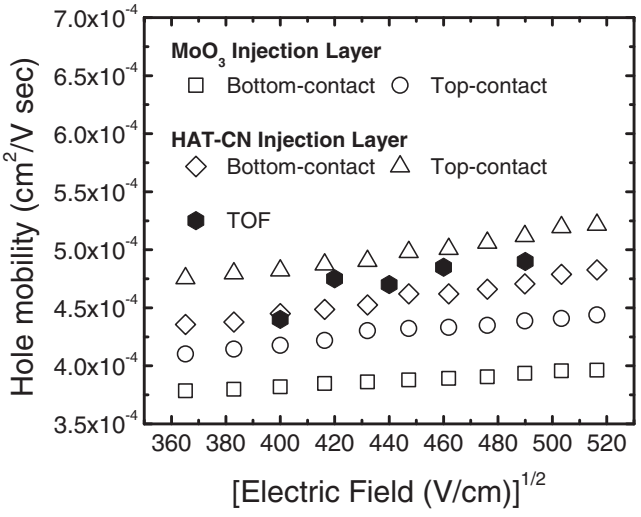

Figure 4. Hole mobility (μ_{DI}) as a function of electric field ($F^{1/2}$) for normal and inverted NPB hole-only device with either MoO_3 or HAT-CN injection layer. Field-dependent mobility based on time-of-flight (TOF) measurements is shown for comparison (with permission from ref. 28).

2.3. MoO_3-doped NPB Injection Layer For Improved Hole Injection

We conjecture that the enhancement in hole injection observed in the inverted devices is attributed to enhanced charge transfer at the top hole-injecting contact. In the inverted device, the electron acceptor dopes the surface and subsurface of the organic semiconductor during thermal evaporation. To confirm that the improved hole injection using electron acceptors as HIL is due to interfacial doping, we fabricated normal structure devices with a 10 nm thick MoO_3 HIL and compared the results to devices with a 10 nm thick NPB:MoO_3 HIL of different doping concentrations. **Figure 5**a and b shows the current density and the hole injection efficiency vs. electric field plots for these devices. As expected, hole injection for the normal NPB device with MoO_3 HIL is contact limited. When the MoO_3 HIL is replaced with a NPB:MoO_3 HIL, significantly larger current densities and enhanced injection efficiencies are obtained. As the doping concentration in the NPB:MoO_3 HIL is increased from 1–10 mol%, the hole injection efficiency is greatly increased at high fields. The difference in hole injection for these devices is due to the degree of surface and subsurface doping occurring at the bottom hole-injecting contact. With MoO_3 as a HIL, the surface layer of NPB is *p*-doped due to the charge transfer at the MoO_3/NPB interface.[29,30] By doping the entire HIL with MoO_3, the resulting heavily *p*-doped NPB enables the formation of ohmic contacts for enhanced hole injection.

This interfacial doping model characterized by the surface and subsurface doping of NPB when using electron acceptors as HIL also applies to our results for HAT-CN assuming that this electron acceptor serves as a *p*-type dopant. Based on the results of our injection study, HAT-CN provides stronger surface and subsurface doping of NPB compared to MoO_3 when used as an injection layer. To compare the *p*-type doping of NPB due to MoO_3 and HAT-CN, we fabricated MoO_3–doped

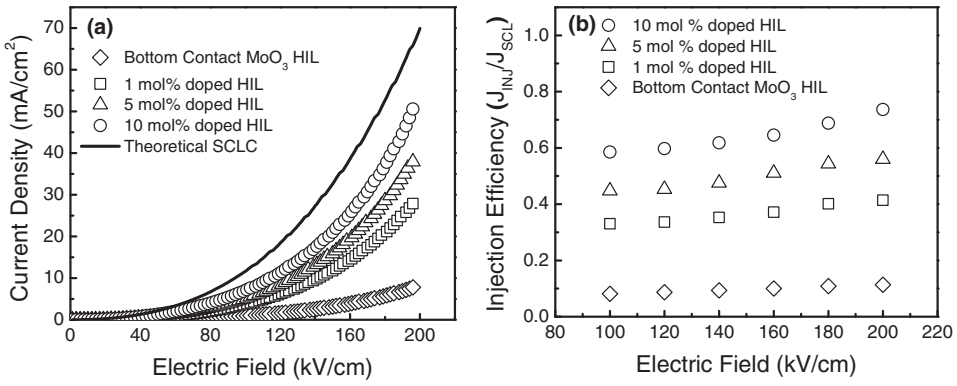

Figure 5. a) Current density vs. applied electric field and b) hole injection efficiency plots for normal NPB hole-only devices with either a neat MoO_3 HIL or a MoO_3-doped NPB HIL of varying doping concentration (1, 5, 10 mol%).

and HAT-CN–doped NPB hole-only devices. The same doping concentration (10 mol%) was used for each electron acceptor. The current density-electric field characteristics of these devices are shown in **Figure 6**. The data for an undoped NPB hole-only device with HAT-CN HIL is also shown for comparison. The data for the undoped device shows the transition from ohmic to trap limited to trap-free SCL transport. On the other hand, the HAT-CN–doped NPB devices show only trap-free SCL transport over the entire voltage range with a current density 3 orders of magnitude larger than the undoped device in the ohmic regime. Compared to the HAT-CN device, the MoO_3–doped NPB device shows the transition from trap limited transport to trap-free SCL transport with a current density at low fields substantially lower than that of the HAT-CN–doped NPB device. These results show a clear indication of *p*-type doping effect of NPB using HAT-CN as dopant which is significantly stronger than that of the devices with MoO_3 doped layer, confirming that HAT-CN provides stronger charge transfer with NPB when used as a dopant compared to MoO_3. When used as a hole injector, HAT-CN would therefore provide stronger interfacial doping of NPB compared to MoO_3 and allow for more efficient charge injection in OLED devices. Based on these results, we conclude that both MoO_3 and HAT-CN injection layers rely on efficient surface and subsurface doping of NPB to form an ohmic contact for hole injection.

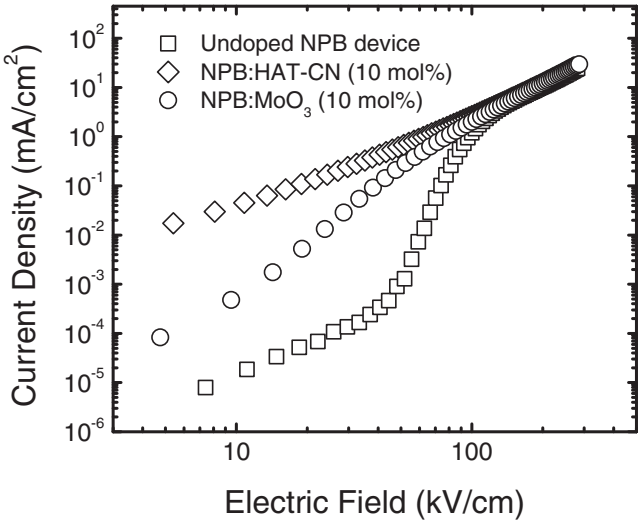

Figure 6. Current density vs. applied electric field plots for MoO3–doped and HAT-CN–doped NPB single carrier devices. Doping concentration was held constant at 10 mol% for both electron acceptors. The data for an undoped NPB hole-only device with HAT-CN HIL is shown for comparison.

Lastly, we recognize that the anode/electron acceptor interface could play a critical role in the results reported in this work. To address the issue of whether the metal/electron acceptor interface contributed to the injection efficiencies of the NPB single-carrier devices, we compared the hole current densities for normal devices with HAT-CN HIL and either Au or ITO as anode. Interestingly, the measured current densities for the devices were independent of the electrode used for the device (see Supporting Information, Figure S2). This result is in agreement with previous studies on metal/electron acceptor interfaces, which showed that the strong charge transfer between the electron acceptor and the anode leads to a lowering of the interfacial energy barrier.[31,32] The work function of the anode becomes pinned to the Fermi level of the electron acceptor, with this Fermi-level pinning being observed for ITO and various metals when paired with an electron accepting HILs.[33] This phenomenon is independent of the device architecture employed, since the degree of charge transfer between the anode and the electron acceptor is very strong.[10–11] Based on these findings, we confirmed that the interfacial doping of NPB at the NPB/electron acceptor interface is responsible for the enhanced hole injection in inverted NPB devices.

3. Conclusions

In conclusion, we demonstrated enhanced hole injection in inverted NPB hole-only devices by using electron acceptors as HIL. *J–V* and DI-SCLC transient measurements were performed to cross-examine the hole injection behavior in normal and inverted NPB hole-only devices. The enhanced hole injection in the inverted hole-only devices was due to enhanced charge transfer at the NPB/electron accepting HIL interface. An interfacial doping model was then proposed to explain the results obtained for the normal and inverted

devices. By utilizing MoO_3-doped NPB HILs, we demonstrated that the hole injection in the normal NPB device can be further enhanced. Increasing the doping concentration of the MoO_3-doped NPB HIL directly increased the injection efficiency, highlighting the importance of interfacial doping to obtain an ohmic contact using these electron acceptors. Lastly, we showed that a strong degree of charge transfer between the HAT-CN and NPB was responsible for the large injection efficiencies obtained in devices with HAT-CN injection layer.

4. Experimental Section

Device Fabrication: Hole-only devices were fabricated by thermal evaporation of the organic small-molecule materials and MoO_3. MoO_3 (99.999% purity) and HAT-CN were used for this study. For the *J–V* and DI-SCLC transient measurements, the following hole-only devices were fabricated: (a) ITO/electron accepting HIL (10 nm)/NPB (1.5 μm)/Au (normal device) and (b) ITO/NPB (1.5 μm)/electron accepting HIL (10 nm)/Au (inverted device). Both devices were fabricated in the same thermal evaporation run for ease of comparison. Prior to film deposition, pre-patterned ITO-coated glass substrates were cleaned by sequential baths of de-ionized water, acetone, and isopropanol. The substrates were then exposed to UV-ozone treatment for 15 minutes. The electron accepting HILs and NPB were thermally evaporated at a base pressure ~10^{-6} Torr onto the substrates at rates of 0.05 and 0.5 nm/s, respectively. The high work function (WF) metal Au was used as the electron blocking cathode in the normal device and as the anode in the inverted device. It should be noted that UV-ozone treated ITO (WF ~ 4.7 eV) served as an effective electron blocking cathode in the inverted device. To compare the quality of hole injection for a neat MoO_3 hole injection layer versus a MoO_3-doped NPB hole injection layer, the following hole-only devices were fabricated simultaneously: (c) ITO/MoO_3 (10 nm)/NPB (1.8 μm)/Au, and (d) ITO/NPB:MoO_3 (10 nm, 1-10 mol%)/NPB (1.8 μm)/Au. For *p*-doped NPB single carrier devices, the doping concentration (10 mol%) was held fixed for both MoO_3–doped and HAT-CN–doped NPB films.

Device Characterization: After fabrication, the *J–V* measurements were performed on the devices in the ambient using a test-fixture connected to a computer-controlled Keithley 4200-SCS. For the DI-SCLC measurements, a pulse generator [HP model 214B] was used to inject holes into the samples by application of a voltage pulse. A digital oscilloscope captured the voltage across a current-sensing resistor that was connected in series to the samples and the corresponding current density was calculated following the measurement.

Supporting Information

Supporting Information is available from the Wiley Online Library or from the author.

Acknowledgements

The authors acknowledge the support of the Department of Energy Basic Energy Sciences (FG0207ER46464).

Received: January 19, 2012
Revised: January 27, 2012
Published online: April 24, 2012

[1] S. Reineke, F. Lindner, G. Schwartz, N. Seidler, K. Walzer, B. Lussem, K. Leo, *Nature* **2009**, *459*, 234.
[2] P. K. Ho, J. S. Kim, J. H. Burroughes, H. Becker, S. F. Y. Li, T. M. Brown, F. Cacialli, R. H. Friend, *Nature* **2000**, *404*, 481.
[3] S. A. VanSlyke, C. H. Chen, C. W. Tang, *Appl. Phys. Lett.* **1996**, *69*, 2160.
[4] A. C. Arias, M. Granström, K. Pertritsch, R. H. Friend, *Synth. Met.* **1999**, *102*, 953.
[5] W. H. Kim, A. J. Mäkinsen, N. Nikolov, R. Shashidar, H. Kim, Z. H. Kafafi, *Appl. Phys. Lett.* **2002**, *80*, 3844.
[6] S. Choulis, V. Choong, A. Patwardhan, M. Mathai, F. So, *Adv. Funct. Mater.* **2006**, *16*, 1075.
[7] K. R. Choudhury, J. Lee, N. Chopra, A. Gupta, X. Jiang, F. Amy, F. So, *Adv. Funct. Mater.* **2009**, *19*, 491.
[8] S. Tokito, K. Noda, Y. Taga, *J. Phys. D: Appl. Phys.* **1996**, *29*, 2750.
[9] Irfan, H. Ding, Y. Gao, C. Small, D. Y. Kim, J. Subbiah, F. So, *Appl. Phys. Lett.* **2010**, *96*, 243307.
[10] S. M. Park, Y. H. Kim, Y. Yi, H.-Y. Oh, J. W. Kim, *Appl. Phys. Lett.* **2010**, *97*, 063308.
[11] Y.-K. Kim, J. W. Kim, Y. Park, *Appl. Phys. Lett.* **2009**, *94*, 063305.
[12] X. Zhou, J. Blochwitz, M. Pfeiffer, A. Nollau, T. Fritz, K. Leo, *Adv. Funct. Mater.* **2001**, *11*, 310-314.
[13] W. Gao, A. Kahn, *Org. Electron.* **2002**, *3*, 53-63.
[14] M. Pfieffer, S. R. Forrest, K. Leo, M. E. Thompson, *Adv. Mater.* **2002**, *14*, 1633-1636.
[15] C. C. Chang, M. T. Hsieh, J. F. Chen, S. W. Hwang, C. H. Chen, *Appl. Phys. Lett.* **2006**, *89*, 253504.
[16] M. Kröger, S. Hamwi, J. Meyer, T. Riedl, W. Kowalsky, A. Kahn, *Org. Electron.* **2009**, *10*, 932.
[17] J. Ma, X. Y. Jiang, Z. Liang, J. Cao, X. Zhang, Z. L. Zhang, *Semicond. Sci. Technol.* **2009**, *24*, 035009.
[18] J. Drechsel, M. Pfeiffer, X. Zhou, A. Nollau, K. Leo, *Synth. Met.* **2002**, *127*, 201.
[19] a) D. Poplavsky, W. Su, F. So, *J. Appl. Phys.* **2005**, *98*, 014501; b) M. Abkowitz, J. S. Facci, J. Rehm, *J. Appl. Phys.* **1998**, *83*, 2670.
[20] C. H. Cheung, W. J. Song, S. K. So, *Org. Electron.* **2010**, *11*, 89.
[21] T.-H. Han, Y. Lee, M.-R. Choi, S.-H. Woo, S.-H. Bae, B. H. Hong, J.-H. Ahn, T.-W. Lee, *Nat. Photon.* **2012**, *6*, 105.
[22] D. Kabra, L. P. Lu, M. H. Song, H. J. Snaith, R. Friend, *Adv. Mater.* **2010**, *22*, 3194.
[23] C. Adachi, K. Nagai, N. Tamoto, *Appl. Phys. Lett.* **1995**, *66*, 2679.
[24] S. C. Tse, S. W. Tsang, S. K. So, *J. Appl. Phys.* **2006**, *100*, 063708.
[25] C. H. Cheung, K. K. Tsung, K. C. Kwok, S. K. So, *Appl. Phys. Lett.* **2008**, *93*, 083307.
[26] P. N. Murgatroyd, *J. Phys. D* **1970**, *3*, 151.
[27] M. A. Lampert, P. Mark, in *Current Injection in Solids*, Academic, New York **1970**.
[28] S. W. Tsang, S. C. Tse, K. L. Tong, S. K. So, *Org. Electron.* **2006**, *7*, 474.
[29] G. Parthasarathy, C. Shen, A. Kahn, S. R. Forrest, *J. Appl. Phys.* **2001**, *89*, 4986.
[30] C. M. Hsu, W. T. Wu, *Appl. Phys. Lett.* **2004**, *85*, 840.
[31] S. Han, Y. Yuan, Z.-H. Lu, *J. Appl. Phys.* **2006**, *100*, 074504.
[32] N. Hayashi, H. Ishii, Y. Ouchi, N. Seki, *J. Appl. Phys.* **2002**, *92*, 3784.
[33] M. G. Helander, Z. B. Wang, Z. H. Lu, *Proc. SPIE* **2008**, *7051*, 70510Z-1.